

OPEN

Multiphoton NAD(P)H FLIM reveals metabolic changes in individual cell types of the intact cochlea upon sensorineural hearing loss

Paromita Majumder^{1,5*}, Thomas S. Blacker^{2,3,4,5*}, Lisa S. Nolan¹, Michael R. Duchon² & Jonathan E. Gale^{1,2}

An increasing volume of data suggests that changes in cellular metabolism have a major impact on the health of tissues and organs, including in the auditory system where metabolic alterations are implicated in both age-related and noise-induced hearing loss. However, the difficulty of access and the complex cyto-architecture of the organ of Corti has made interrogating the individual metabolic states of the diverse cell types present a major challenge. Multiphoton fluorescence lifetime imaging microscopy (FLIM) allows label-free measurements of the biochemical status of the intrinsically fluorescent metabolic cofactors NADH and NADPH with subcellular spatial resolution. However, the interpretation of NAD(P)H FLIM measurements in terms of the metabolic state of the sample are not completely understood. We have used this technique to explore changes in metabolism associated with hearing onset and with acquired (age-related and noise-induced) hearing loss. We show that these conditions are associated with altered NAD(P)H fluorescence lifetimes, use a simple cell model to confirm an inverse relationship between τ_{bound} and oxidative stress, and propose such changes as a potential index of oxidative stress applicable to all mammalian cell types.

The World Health Organization estimates that over 5% of the world's population suffer from a disabling hearing impairment¹. Acquired sensorineural hearing loss (SNHL) accounts for approximately 90% of these cases², with the most common being the noise-induced (NIHL) and age-related (ARHL) conditions. The vulnerability of cochlear sensory hair cells to trauma and, more recently, the associated loss of cochlear nerve fibres are together believed to be the major causes of SNHL³. The contribution of cellular metabolism to this vulnerability is now becoming established^{4–10}, guiding attempts at therapeutic intervention¹¹. Given the highly heterogeneous cell population present in the sensory organ of the cochlea, the organ of Corti, conventional whole-tissue analyses will fail to reveal which cell types are critical to the pathophysiology. A full understanding of the role of altered metabolism in hearing loss therefore requires experimental approaches capable of interrogating intact cochlear preparations with cellular resolution. Here, we have used fluorescence lifetime imaging microscopy (FLIM) to observe cell-specific metabolic responses in the reduced pool of the metabolic cofactor nicotinamide adenine dinucleotide (NADH) and its phosphorylated analogue NADPH in response to hearing development, maturation and its noise-induced and age-related loss. The measurements motivate the development of a framework for interpreting the results of NAD(P)H FLIM experiments in terms of oxidative stress phenotypes, raising novel questions regarding the metabolic roles of individual cell types in the health and disease of the auditory system.

FLIM extends conventional laser scanning techniques to measure the rate of excited state depopulation at each pixel of an image. This photophysical property, known as the fluorescence lifetime, is altered by changes to the nanoscale local environment of a molecule, thus making FLIM a highly sensitive probe of intracellular biochemistry when applied to the intrinsic fluorescence of living samples¹². The spectrally-identical autofluorescence

¹UCL Ear Institute, University College London, Grays Inn Road, London, WC1X 8EE, UK. ²Research Department of Cell & Developmental Biology, University College London, Gower Street, London, WC1E 6BT, UK. ³Department of Physics & Astronomy, University College London, Gower Street, London, WC1E 6BT, UK. ⁴Centre for Mathematics and Physics in the Life Sciences and Experimental Biology, University College London, Gower Street, London, WC1E 6BT, UK. ⁵These authors contributed equally: Paromita Majumder and Thomas S. Blacker. *email: paromita.majumder@gmail.com; t.blacker@ucl.ac.uk

of NADH and NADPH is often used for this purpose^{13–17}. Both cofactors carry reducing equivalents within the cell but are involved in distinct metabolic pathways¹⁸. The NAD pool participates primarily in ATP-generating catabolic processes, linking the citric acid cycle to the electron transport chain (ETC) in the mitochondria and regulating the rate of glycolysis in the cytosol. In contrast, NADP is involved in anabolic reactions such as lipid and nucleic acid synthesis and, importantly, in maintaining the glutathione and thioredoxin reductase antioxidant defence systems¹⁵. The widespread links between altered metabolism and disease have driven the use of NAD(P)H FLIM to investigate these processes in a variety of living cell and tissue models^{19–23}.

Free in solution, the fluorescence lifetimes of NADH and NADPH are identical²⁴. For either molecule, two species with distinct lifetimes of 0.3 ns and 0.7 ns are observed in aqueous environments, which likely result from alternate configurations of their nicotinamide ring²⁵. Inside cells, NAD(P)H emission with a lifetime of 0.4 ns is typically observed, likely reflecting an equilibrium between these two freely-diffusing states, alongside a longer lifetime component which arises through binding of the cofactors to enzymes¹⁵. NAD(P)H FLIM measurements therefore report three fluorescence decay parameters at each pixel of an image: the shorter lifetime of free NAD(P)H in solution τ_{free} , the longer average lifetime of the enzyme-bound species present at that pixel τ_{bound} , and the proportion of the NAD(P)H at that pixel which is enzyme bound α_{bound} ¹³. The quantities τ_{bound} and α_{bound} have been observed to differ in response to metabolic perturbation and the onset of disease, prompting diagnostic tools to be designed based on time-resolved autofluorescence methods²⁶. Indeed, these techniques have previously been applied to investigate the metabolism of the cochlea^{19,27}. However, their full potential has yet to be realised as the interpretation of the nanoscale properties reported by the NAD(P)H fluorescence decay in terms of the underlying physiological or biochemical state of the tissue has not yet been unambiguously defined^{14–17}.

In our previous work, we sought to understand the biochemical relevance of changes in τ_{bound} ¹⁹. We demonstrated that this parameter reflects the ratio of [NADPH] to [NADH], as NADPH exhibits a longer fluorescence lifetime than NADH when bound to enzymes within cells. This has allowed us to separately interrogate these functionally-distinct pools using fluorescence techniques for the first time^{28–30}. In immature cochlear explant cultures, we measured significantly larger values of τ_{bound} in pillar cells, suggesting locally increased [NADPH]/[NADH] ratios, and we showed that this was associated with enrichment of reduced glutathione (GSH) in those cells^{19,31}. The present study is a direct extension of that work, now applying NAD(P)H FLIM in the intact cochlea to investigate metabolic contributions to the pathophysiology of NIHL and ARHL.

Results

Noise exposure decreases bound NAD(P)H lifetime in both hair cells and pillar (supporting) cells in the organ of Corti.

We compared NAD(P)H FLIM measurements in intact bulla preparations from adult mice (3 weeks old) that had or had not been subject to 100 dB octave-band (8–16 kHz) noise for 2 hours, a noise exposure protocol that elicits a temporary threshold shift (TTS) that persists for at least a day following treatment³². We segmented the metabolic responses into the primary functional cells of the organ of Corti shown in Fig. 1A: sensory inner hair cells (IHCs), that convert the mechanical sound stimulus into a nerve signal, sensori-motor outer hair cells (OHCs), which play a role in amplifying this response, and the non-sensory inner and outer pillar cells (IPCs and OPCs) which play structural and trophic roles to support hair cell function^{31,33}.

In line with our previous work, we observed that values of τ_{bound} under control conditions were significantly ($P = 10^{-19}$) longer in pillar cells than in hair cells, at $3.24(\pm 0.07)$ ns in OPCs (57 cells across 4 repeats) and IPCs (52 cells) compared to $3.00(\pm 0.10)$ ns and $3.12(\pm 0.09)$ ns in OHCs (90 cells) and IHCs (33 cells) respectively. The mild noise exposure caused a significant decrease in τ_{bound} in all four cell types (Fig. 1B–D). The extent of the decrease was larger in the IHCs (6%, $P = 10^{-7}$, 46 cells across 4 repeats) and IPCs (8%, $P = 10^{-17}$, 70 cells) than the OHCs (5%, $P = 10^{-11}$, 158 cells) and OPCs (2%, $P = 10^{-4}$, 89 cells).

Combining the fluorescence decay parameters with the total intensity changes following noise exposure (Fig. 2A) using established procedures^{13,19,34} allowed the differing responses of the NADH and NADPH pools to be determined. Using this approach, we found that the large decrease in τ_{bound} in the IHCs and IPCs upon noise exposure reflected a significant increase in NADH, rather than a decrease in NADPH, relative to the OPCs (Fig. 2B,C).

Changes in bound NAD(P)H lifetime show distinct patterns between hair cells and pillar cells during maturation of the hearing system.

In rodents at birth, the organ of Corti is not fully mature, supporting cells are not fully differentiated and sensory hair cells are not fully functional. Hearing onset begins after ~12 days, at which point the hair cell synapses are well formed, the endocochlear potential is established and the tunnel of Corti, bounded by the inner and outer pillar cells, has formed³³. These features become fully mature by one month. While many mouse strains may maintain hearing up to 2 years of age, in the C57BL/6 strain studied here, accelerated cochlear degeneration leads to almost complete deafness by this point³⁵, thus providing a well-established model to monitor metabolic changes in the cells of the organ of Corti during post-natal development and with age. We performed NAD(P)H FLIM on cochlear preparations of one week (1 W), two weeks (2 W), three weeks (3 W), one month (1 M), one year (1 Y) and two years (2 Y) of age. These data are shown in Fig. 3, with numerical values available in Supplementary Material Table S1.

At 1 W, in contrast to our previous work in immature rat cochlear explant cultures¹⁹, the pillar cells did not exhibit the highest τ_{bound} . At $2.90(\pm 0.08)$ ns, this parameter was equal in OHCs, OPCs and IPCs, with a significantly larger value in the IHCs at $3.00(\pm 0.20)$ ns ($P = 10^{-5}$). As hearing developed between 1 W and 2 W, τ_{bound} changed in the opposite direction in the hair cells and pillar cells, decreasing to $2.78(\pm 0.06)$ ns in OHCs ($P = 10^{-7}$) and to $2.91(\pm 0.09)$ ns in IHCs ($P = 0.008$) but increasing to $3.03(\pm 0.08)$ ns in OPCs ($P = 10^{-6}$) and $3.01(\pm 0.08)$ ns in IPCs ($P = 0.002$). From 2 W to 3 W, the enzyme-bound lifetime increased in all cell types ($P = 10^{-5}$), establishing the pattern we observed previously of larger τ_{bound} in OPCs and IPCs than in the OHCs and IHCs. In contrast, τ_{bound} decreased in all cell types between 3 W and 1 M ($P = 0.02$), indicating possible redox

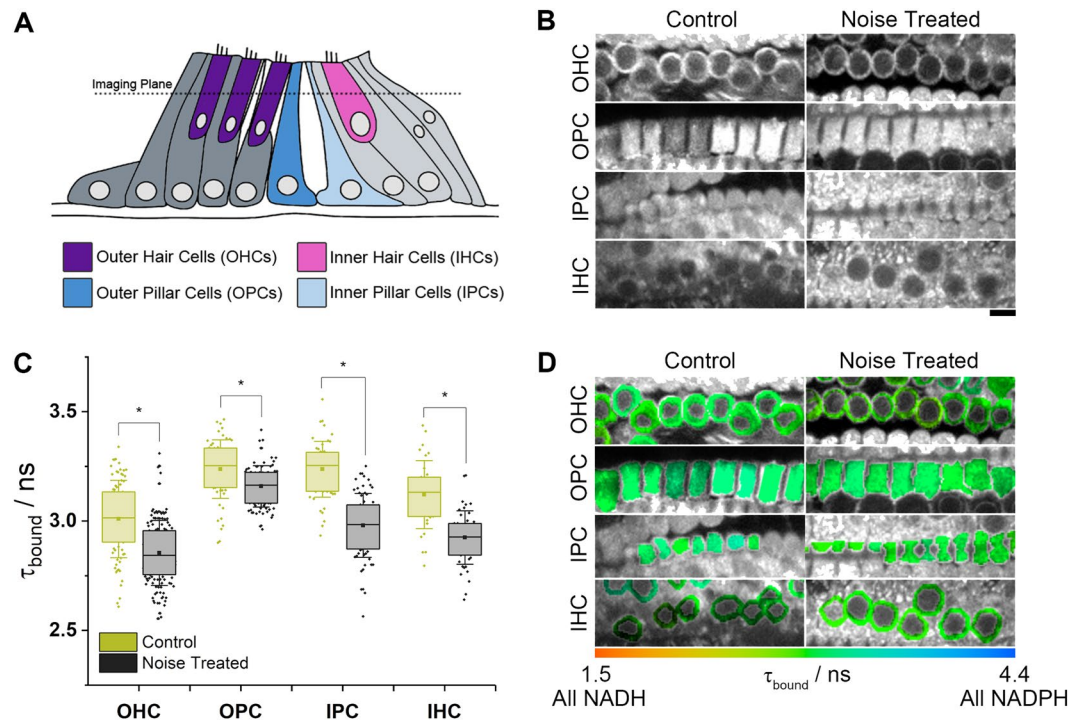


Figure 1. Noise treatment causes a decrease in τ_{bound} in both sensory and supporting cells of the organ of Corti. **(A)** Schematic of the organ of Corti, showing the four cell types investigated in this work. **(B)** NAD(P)H fluorescence intensity images of cochlea preparations from three week old (P21–23) mice exposed to mild (TTS) noise treatment (2 hours at 100 dB SPL) compared to control (unexposed) conditions (scale bar 10 μm). **(C)** Mean enzyme bound NAD(P)H fluorescence lifetimes of each cell type (* $P < 10^{-4}$). **(D)** FLIM images colour coded to the mean τ_{bound} value in each cellular region of interest.

adjustments upon maturation, before remaining constant between 1 M and 1 Y. Development therefore appeared to be accompanied by a significant metabolic switch³⁶, before the redox state settled throughout adulthood.

τ_{bound} decreased in OPCs, IPCs and IHCs by an average of 6% ($P < 0.005$) between 1 Y and 2 Y but remained constant in OHCs. However, the validity of the OHC data at this time point in these cells is debatable due to their significant loss by this time in the C57BL/6 strain^{37,38}, resulting in only 11 surviving cells being imaged across 10 repeats. For other cell types and ages, the number of cells included in each reported mean are included for reference in Supplementary Material Table S1.

Calculating the relative concentrations of NADH and NADPH in each cell type at each age (Fig. 4), OHCs consistently displayed the lowest NADH levels of the four cell types and the pillar cells the highest. Changes in NADPH levels typically mirrored those of NADH.

Bound NAD(P)H lifetime may act as an intrinsic indicator of oxidative stress. In accordance with our previous work¹⁹, changes in τ_{bound} have been interpreted as changes in the relative levels of NADH and NADPH. However, it is the NAD^+/NADH and $\text{NADP}^+/\text{NADPH}$ redox ratios, rather than the absolute levels of their reduced forms, which are the drivers of the biochemical pathways they regulate³⁹. As such, it would be more convenient to be able to understand changes in τ_{bound} in terms of the wider metabolic phenotype.

We previously observed correlations between the high τ_{bound} values measured in the pillar cells and increased GSH levels¹⁹. Corresponding GSH measurements at 2 W, 1 M and 1 Y showed a similar relationship, with an R^2 correlation coefficient of 0.6 across the four cell types measured (Fig. 5A). The positive correlation suggested that the antioxidant defence level of the system is partially reflected in the measurement of τ_{bound} . However, as R^2 was significantly less than one, it is likely that τ_{bound} may yet be linked to additional aspects of metabolic state.

A further cellular-level property that may determine the enzyme bound NAD(P)H lifetime can be surmised by considering the contrasting principal roles of NADH and NADPH. The systems for neutralising reactive oxygen species (ROS) inside cells are regulated by NADPH⁴⁰. Given the relationship between $[\text{NADPH}]$, $[\text{NADH}]$ and τ_{bound} ¹⁹, the observed positive correlation between τ_{bound} and antioxidative capacity is expected. Conversely, high NADH levels drive the production of superoxide, the proximal mitochondrial ROS, by the ETC⁴¹. With the latter, a negative correlation between τ_{bound} and the level of ROS production is predicted. The enzyme bound NAD(P)H lifetime may thus reflect the balance between ROS defence and production, an established metabolic phenomenon known as oxidative stress¹⁵.

To investigate the possibility of an inverse relationship between τ_{bound} and oxidative stress, we performed experiments in simple cell models. Oxidative stress can be increased by increasing the rate of ROS generation or by depleting antioxidative capacity⁴². In HEK293 cells, chronic low-dose rotenone treatment was used to increase

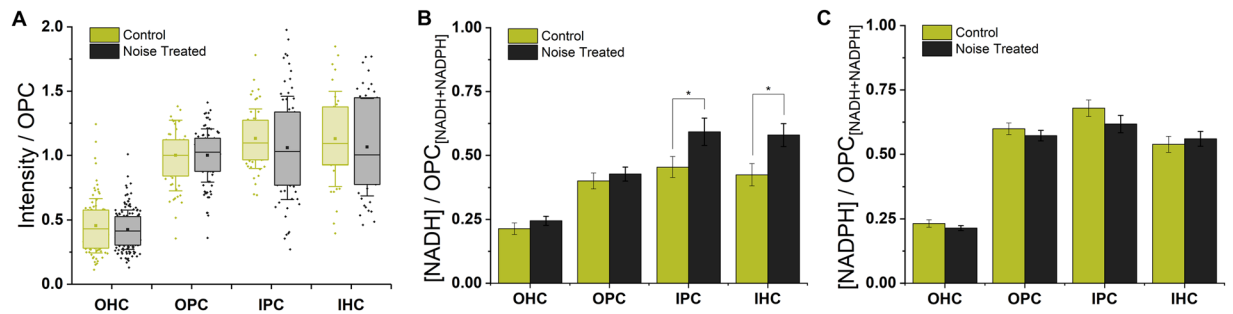


Figure 2. Noise-induced decreases in τ_{bound} in IHCs and IPCs result from an increase in NADH in these cells relative to OPCs. (A) NAD(P)H fluorescence intensity of each cell type under control and noise-treated conditions, normalised in each image to the mean OPC level. These cells were the most metabolically stable population following noise exposure, based on the smallest changes in NAD(P)H fluorescence decay parameters. (B,C) Corresponding NADH and NADPH concentrations, again relative to OPCs, calculated using established procedures³⁴ from the fluorescence intensity and decay parameters.

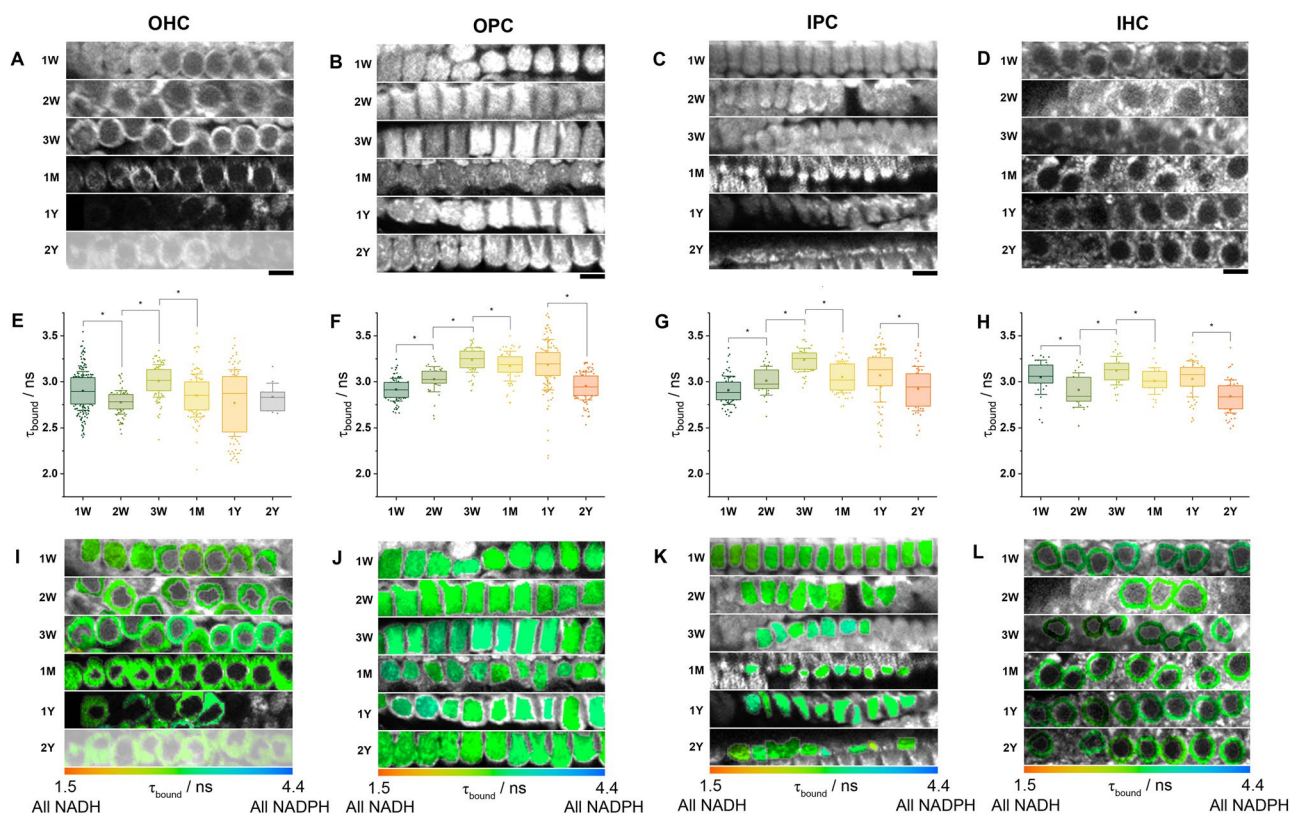


Figure 3. Development and ageing cause distinct patterns of τ_{bound} variation in HCs and PCs. (A–D) NAD(P)H fluorescence intensity images of each cell type at varying postnatal ages (scale bar 10 μm). (E–H) Mean enzyme bound NAD(P)H fluorescence lifetimes τ_{bound} (* $P < 0.05$). (I–L) FLIM images colour coded for the mean τ_{bound} value in each cellular region of interest. OHC data is truncated at 1Y due to early-onset hearing loss in C57BL/6 mice.

the production of ROS by the ETC⁴³, and BSO was used to deplete GSH⁴⁴. DHE staining was used to confirm that both treatments increased oxidative stress, with the baseline rate of oxidation increasing by 16(\pm 5)% ($P = 0.04$) and 23(\pm 6)% ($P = 0.02$) in the presence of rotenone and BSO respectively (Fig. 5B,C). With both treatments, τ_{bound} was observed to decrease, in support of our proposal. Rotenone caused a decrease of 0.33(\pm 0.06) ns (13%, $P < 10^{-6}$) and BSO a decrease of 0.15(\pm 0.05) ns (6%, $P = 0.001$) as shown in Fig. 5D.

Conversely, to investigate whether increased τ_{bound} values correlated with decreased oxidative stress, we repeated the DHE measurements on HEK293 cells in which the enzyme NAD kinase had been overexpressed⁴⁵. We previously observed this perturbation to cause greatly enhanced enzyme bound NAD(P)H fluorescence

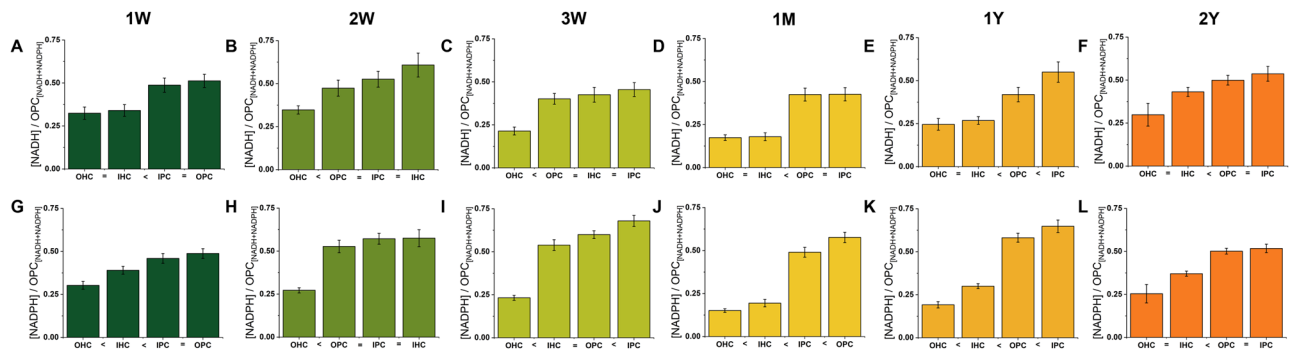


Figure 4. OHCs consistently display the lowest levels of both NADH and NADPH. By combining the NAD(P)H fluorescence intensities and decay parameters using established procedures³⁴, internal comparisons between cell types of the absolute NADH (A–F) and NADPH (G–L) levels could be made at each postnatal age. Differences (<) between cell types were taken as $P < 0.05$. NADPH levels were typically highest in the pillar cells.

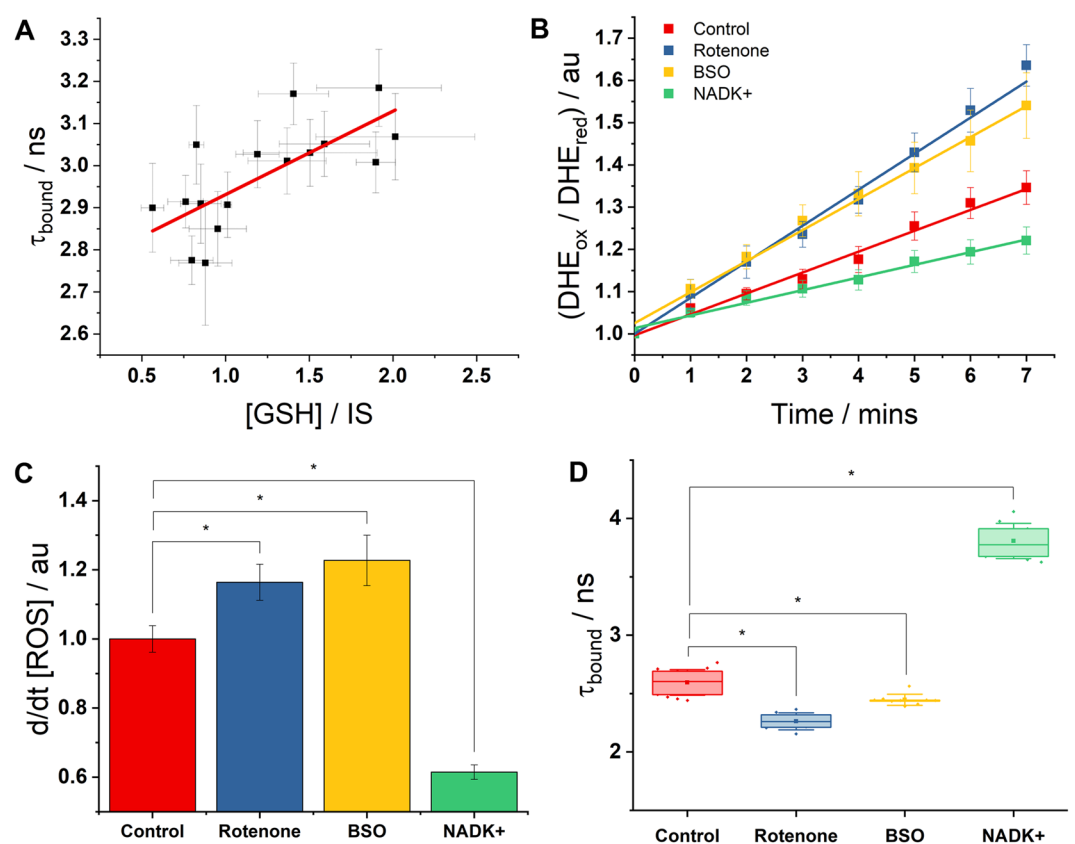


Figure 5. τ_{bound} exhibits an inverse correlation with oxidative stress in HEK293 cells. (A) Using monochlorobimane (MCB) imaging, the levels of reduced glutathione (normalised to inner sulcus, IS, as previously³¹) in each cell type at 2W, 1M and 1Y time-points showed a minor correlation ($R^2 = 0.6$) with the corresponding enzyme-bound NAD(P)H fluorescence lifetime data, suggesting that the antioxidative capacity of a system contributes, in part, to the value of τ_{bound} measured. (B,C) Culturing cells for 24 hours in rotenone (200 nM) or BSO (100 μM) each caused a significant increase in oxidative stress, based on the rate of DHE oxidation. Overexpression of NAD kinase (NADK+) caused this quantity to decrease ($*P < 0.05$). (D) Changes in oxidative stress were mirrored by opposite changes in τ_{bound} ($*P < 0.001$). NADK+ fluorescence lifetime data was taken from previous work¹⁹.

lifetimes of $3.81(\pm 0.09)$ ns¹⁹. In line with our hypothesis, the rate of DHE oxidation in these cells was greatly decreased, by $39(\pm 2)\%$ relative to control ($P = 0.001$).

NAD kinase overexpression increases the level of NADPH but not NADH⁴⁵, increasing the antioxidative capacity of the cells and the values of τ_{bound} measured from them¹⁹. Using the fluorescence decay parameters

and NAD(P)H fluorescence intensity measurements, we calculated the corresponding changes in NADH and NADPH concentrations following rotenone and BSO treatment (Supplementary Material Fig. S5). We observed that τ_{bound} decreased following rotenone application due primarily to a 37(\pm 8)% increase in NADH ($P = 0.0003$), whereas it decreased following BSO due to a 23(\pm 4)% decrease in NADPH ($P = 0.002$). These data provide the first direct evidence of a convenient relationship between changes in the relative concentration of these two cofactors and the resulting impacts on both the physiological state of oxidative stress and the NAD(P)H fluorescence decay parameter τ_{bound} .

Discussion

The sensory hair cells and phalangeal pillar cells are traditionally known as the prime targets of noise exposure^{46,47}, although recent data has shown that mild noise exposure can also result in partial loss of auditory nerve fibre (ANF) connections with IHCs⁴⁸. The mechanical activity associated with the sound-induced movements of the organ of Corti is likely to put both the sensory hair cells and structural supporting cells under significant metabolic stress during prolonged noise exposure (i.e. “auditory ageing”). Such metabolic effects are consistent with our observed changes in the enzyme bound NAD(P)H fluorescence lifetime measured in noise-exposed excised bulla preparations in each cell type. This could indicate a common stress mechanism, perhaps as a result of mechanical trauma or due to the propagation of changes in cellular redox state from hair cells to support cells, possibly via intercellular calcium signalling that we have previously described^{49–51}. Moreover, intercellular metabolite exchange has previously been demonstrated between different cells in the brain⁵² in the export of GSH by astrocytes for uptake by neurons⁵³. This has recently been shown to be mirrored in the cochlea, where supporting cells are thought to contribute to the detoxification of cochlear ROS by releasing GSH through Cx26 hemichannels⁵⁴.

In hair cells, pathological noise exposure caused similar changes as observed around the onset of hearing, i.e. when sound first enters the cochlea³¹, with τ_{bound} decreasing between the first and second postnatal weeks. The cochlear data herein are consistent with our proposal that a decrease in enzyme bound NAD(P)H fluorescence lifetime reflects an increase in oxidative stress in cochlear cells. Firstly, as τ_{bound} decreased in all cell types from 3 W (maturity) to 2 Y (aged), this correlation would be consistent with theories of ageing based on depletion of antioxidant systems and accumulation of ROS mediated damage⁵⁵. Secondly, the steady increase in τ_{bound} in the pillar cells during post-natal maturation of the cochlea is consistent with an increasing expression of antioxidant enzymes observed in brain tissue over the course of postnatal development^{56–58}. Finally, as sound exposure causes mechanical and metabolic effects in both hair cells and supporting cells, the acute and marked decrease in τ_{bound} in hair cells exposed to sound could reflect the lipid peroxidation, and resulting excess ROS generation, described upon acoustic overstimulation⁵⁹. NAD(P)H FLIM may therefore provide a suitable technique for the assessment of antioxidant therapies for arresting SNHL.

Linking τ_{bound} to oxidative stress can also provide further insight into existing NAD(P)H FLIM studies. For example, the frequently-observed shortening of the enzyme bound lifetime in cancer relative to healthy tissue^{17,60–62} could reflect the increase in oxidative stress thought to drive oncogenesis⁶³, and our recent observation of diabetic pancreatic islets exhibiting a shorter τ_{bound} at low glucose levels than healthy equivalents supports suggestions of increased oxidative stress playing a role in the pathophysiology of this disease⁶⁴. Further, a significant recent advance linking NAD(P)H FLIM measurements to intracellular biochemistry was Schaefer *et al.*'s report of correlations between the mean NAD(P)H lifetime and the pH of the mitochondrial matrix⁶⁵. Specifically, the amplitude-weighted mean lifetime was observed to increase linearly with oxygen consumption rate (OCR), with the constant of proportionality between the two parameters dependent on the matrix pH. Given the definition of the mean lifetime, this constant of proportionality can itself be estimated to be proportional to τ_{bound} (see Supplementary Material, Appendix 2). As superoxide production by the ETC is decreased as mitochondrial pH is lowered⁶⁶, our hypothesis would suggest that the mean lifetime would increase with OCR with a larger constant of proportionality at lower mitochondrial pH. This is precisely what Schaefer *et al.* observed, thereby offering a mechanistic explanation for these correlations.

Despite the successes described, the proposed relationship relies on notional roles of enzyme bound NADH and NADPH as contributing to pro- or anti-oxidant pathways only. A potentially confounding factor in this interpretation is the action of the NADPH oxidases¹⁵, which produce superoxide by directly reducing molecular oxygen using electrons donated by NADPH. In the cochlea, acute noise exposure upregulates the expression of the NOX1 isoform and this is suggested to contribute to noise-induced cochlear injury by increasing oxidative stress⁶⁷. However, we still observed τ_{bound} to decrease under the noise-exposure conditions used herein. An explanation for this could lie in the fast kinetics of the NADPH oxidase enzyme when oxygen is available, in which the cofactor is immediately oxidised by a flavin functional group upon binding, rendering it non-fluorescent and incapable of contributing to the τ_{bound} measurement while the enzyme is producing superoxide⁶⁸. Whether this is occurring in the cochlea remains to be tested.

Conclusion

This work demonstrates the application of NAD(P)H FLIM for monitoring changes in redox-associated metabolism in complex, living tissue samples. We show that metabolic modifications can be identified in different cochlear cell types within 2 hours of mild noise exposure, prior to any overt morphological change of the system, demonstrating the sensitivity of the technique. A decrease in the fluorescence lifetime of enzyme bound NAD(P)H occurred in HCs following noise exposure in both pathological and developmental (onset of hearing) contexts. τ_{bound} then reached a peak during cochlear maturation before decreasing during ageing. These observations, combined with the known roles of NADPH and NADH and their relationship to the NAD(P)H fluorescence decay, strongly suggest changes in τ_{bound} as a new biomarker for changes in oxidative stress. Such a relationship would open new avenues of research in the NAD(P)H FLIM field, such as in the label-free identification of subsets of cell populations that may be resistant to pro-oxidant therapies^{69–72}.

Methods

Noise exposure protocol. C57BL/6 mice (P21–23, $n = 4$) were anesthetized with ketamine (100 mg per kg weight, i.p.) and medetomidine (0.54 mg per kg weight, i.p.) and positioned in a sound proofed booth on a heated pad 45 cm beneath the centre of a speaker (Stage Line PA Horn Tweeter MHD-220N/RD) as described previously³². An RX6 processor (Tucker-Davis Technologies, TDT) generated octave-band noise (8–16 kHz) for 2 hours, attenuated (TDT PA5) and amplified (TDT SA2) to a sound pressure level (SPL) of 100 dB. The speaker was calibrated prior to each use to ensure a flat (± 2 dB) frequency response over this range. Pedal reflex and breathing rate were checked every 30 minutes. Control animals ($n = 4$) were not exposed to any additional sound beyond the normal background noise in the animal unit.

Postnatal auditory bulla preparation. Animals were sacrificed in accordance with the United Kingdom Animals (Scientific Procedures) Act of 1986 using a protocol described previously³¹, approved by the UCL Biological Services Animal Ethics Committee. In addition to the noise exposure experiments, cochlea from 1 week old (P8, $n = 3$), two week old (P15, $n = 3$), one month old (P30, $n = 4$), one year old (P321–381, $n = 8$) and two year old (P553–721, $n = 10$) C57BL/6 mice were collected. Auditory bullae were isolated and transferred into Leibovitz's L15 medium (Thermo Fisher Scientific) and then a window was opened in the apical turn. Reissner's membrane was peeled away and the stria vascularis removed in order to gain visual access to the organ of Corti³¹. While C57BL/6 mice are well known to have a mutation in the cadherin23 gene (Cdh23^{ah1}) that results in an accelerated form of ARHL^{37,38}, we nevertheless consider that the relative changes we describe here for the first time are still particularly relevant as an initial internal description of changes in cellular metabolism with age in both sensory and non-sensory cells in the cochlea.

NAD(P)H FLIM experiments. All experiments were performed using protocols described previously^{13,34} using an upright LSM510 microscope (Carl Zeiss) equipped with a 40 \times (NA 1.0) water-dipping objective. The basal end of the auditory bullae were secured to the bottom of a 35 mm plastic dish with a small drop of superglue and bathed in L15 medium. NAD(P)H was imaged in the apical coil of the preparation using a Ti:sapphire laser (Chameleon Ultra, Coherent) tuned to 720 nm. Fluorescence was detected by a hybrid photomultiplier tube (HPM-100, Becker & Hickl) after passing through a 435–485 nm emission filter. Emission events were registered by a time correlated single photon counting module (SPC-830, Becker & Hickl). Scanning was performed continuously for 2 minutes with a pixel dwell time of 1.6 μ s, resulting in 256 \times 256 (125 μ m \times 125 μ m) FLIM images containing between 10¹ and 10³ photons per pixel. 5 \times 5 binning (2.5 \times 2.5 μ m) was applied to increase pixel signal to noise and least squares fitting of the biexponential decay function

$$I(t) = I(0) \left[(1 - \alpha_{\text{bound}}) \exp\left(-\frac{t}{\tau_{\text{free}}}\right) + \alpha_{\text{bound}} \exp\left(-\frac{t}{\tau_{\text{bound}}}\right) \right] \quad (1)$$

was then performed using SPCImage 3.0.8 (Becker & Hickl) using iterative reconvolution with an instrument response function (IRF) recorded from the 460 nm second harmonic generation signal of a potassium dihydrogen phosphate crystal at 920 nm excitation. In this FLIM system, the pulse arrives 4 ns into the time to amplitude converter (TAC), almost a third of the way through the 12.5 ns period between pulses. An incomplete multiexponential model was therefore used and the fitting limits expanded to incorporate the entire trace at each pixel. This avoided wasting the remaining portion of the fluorescence decay recorded in the lead up to the next pulse. A constant (time-uncorrelated) offset was allowed to float at each pixel to account for background fluorescence and the IRF was translated across the time axis to compensate for its dependence on excitation wavelength. To reduce processing time, the IRF position that minimised the χ^2_R statistic at an arbitrary cytosolic pixel was found and then fixed across the image. Mean parameter values across cellular regions of interest were measured by exporting the data to ImageJ (NIH). NADH and NADPH levels were quantified by combining the fluorescence decay parameters with the total photon counts using previously published procedures¹⁹. Laser powers at the back aperture of the objective were 17(± 1) mW. To account for variations in power at the imaging plane, due either to beam drift or depth of tissue in the beam path, it was necessary to normalise the NAD(P)H concentrations in each image to one cell type in the image window. The outer pillar cells (OPCs) were chosen, being the most metabolically-stable cell type present based on the smallest changes in both τ_{bound} and α_{bound} following noise exposure.

Tissue fixation and immunohistochemistry. The viability of all preparations following the experiments was assessed by immunohistochemistry. After fixation in 4% PFA, all bullae preparations were rinsed three times with PBS and incubated in blocking solution (PBS, 10% secondary host antibody serum, 0.5% Triton X-100) for 2 hours^{31,73}. The bullae were then washed three times with PBS and incubated for 2 hours at room temperature in blocking solution containing 4',6'-diamidino-2-phenylindole (DAPI, 1 μ M) and phalloidin Alexa Fluor 647 nm (33 nM). The quality of the excised bullae preparations were then evaluated by immunofluorescence (see Supplementary Material Fig. S8). Images were acquired using a Zeiss 510NLO upright confocal microscope using the appropriate excitation wavelengths and emission filters (DAPI 720 nm/435–485BP, phalloidin 633 nm/650LP). The images were acquired at 1.5–2 μ m z-intervals using 40x Achromplan (NA 0.8) or 63x Achromplan Vis-IR (NA 1.0) water immersion objectives.

Glutathione measurements. Monochlorobimane (MCB) passes across the cell membrane and forms a fluorescent adduct when combined with GSH in a reaction catalyzed by glutathione S-transferase. Conjugated GSH-MCB fluorescence can therefore be used as a readout of GSH levels^{19,31,44}. After opening, bullae at ages

2W (n = 3), 1M (n = 9) and 1Y (n = 8) were incubated in 50 μ M MCB (Sigma-Aldrich) for 30 minutes. A subset of this now-expanded dataset has been published previously³¹. GSH-MCB was imaged on a Zeiss 510NLO Axioskop using multiphoton excitation from a Chameleon-XR Ti:Sapphire laser (Coherent) tuned to 780 nm and fluorescence emission was captured using a 435–485 nm bandpass filter. Image stacks were acquired at 2 μ m intervals using a 40 \times (NA 0.8) water immersion objective. All experiments were performed at room temperature (20–23 °C) keeping all confocal imaging parameters constant between experiments.

Cell culture models of oxidative stress. HEK293 cells were grown in Advanced Dulbecco's Modified Eagle Medium (DMEM) supplemented with 10% fetal bovine serum, 2 mM GlutaMAX, 100 U ml⁻¹ penicillin and 100 mg ml⁻¹ streptomycin (all Gibco). Additionally, NADK+ cultures¹⁹ were grown in the presence of 0.1 mg ml⁻¹ G418 (Gibco). Cells were grown as monolayers in sterile 75 cm² tissue culture flasks (Thermo Fisher) in a 37 °C, 5% CO₂ incubator. For imaging, a 22 mm diameter coverslip was placed in each well of a six well plate (Thermo Fisher) before adding 3 \times 10⁵ cells per well. Media was changed after 24 hours, when rotenone (final concentration 200 nM) or buthionine-sulfoximine (BSO, final concentration 100 μ M) was added if required. Both stock solutions of the treatments were made up in DMSO, so an equivalent amount of DMSO was added to untreated wells (1 μ l in 2 ml of growth media) as a vehicle control. Coverslips were imaged 24 hours later, held in a custom-made stainless steel ring and bathed in DMEM free of phenol red (Sigma) and buffered by 10 mM HEPES.

For oxidative stress assessment, coverslips were loaded with 5 μ M dihydroethidium (DHE) for 10 minutes before being imaged on an inverted LSM510 confocal microscope (Carl Zeiss) using a 40 \times (1.3 NA) oil immersion objective. DHE exhibits blue cytosolic fluorescence until it is oxidised, whereupon its localisation changes to the nucleus and absorption and emission spectra shift to the red⁷⁴. DHE was excited at 351 nm and imaged using 435–485 nm (blue) emission filters. Oxidised DHE was excited at 543 nm and imaged using a 560 nm (red) long pass filter. 512 \times 512 images were taken every minute and subsequently analysed in ImageJ. Blue and red fluorescence images were each normalised to their initial values before the blue to red ratio time series was calculated. Three repeats were performed for each treatment and seven repeats were performed under vehicle control conditions. The average red to blue (DHE_{ox}/DHE_{red}) ratio time series was determined for each condition by taking a mean across repeats and its rate of increase was calculated using a weighted least squares straight line fit in OriginPro 2015 (MicroCal).

Statistics. Statistical sampling considerations for the FLIM analysis protocol above are described in Supplementary Material Appendix 1. All numerical quantities are reported as mean (\pm SEM), with n as the number of biological repeats for each condition. Statistical significance (P < 0.05) was judged using unpaired Student's t-tests. Box and whisker plots use 25th and 75th percentiles for the boxes and standard deviations for the whiskers. Horizontal lines correspond to the median value and the datapoint within the box reflects the mean.

Data availability

Raw datasets available upon request to corresponding authors.

Received: 1 July 2019; Accepted: 27 November 2019;

Published online: 11 December 2019

References

1. Olusanya, B. O., Neumann, K. J. & Saunders, J. E. The global burden of disabling hearing impairment: a call to action. *Bull. World Health Organ.* **92**, 367–373 (2014).
2. Smith, R. J. H., Bale, J. F. Jr. & White, K. R. Sensorineural hearing loss in children. *Lancet* **365**, 879–890 (2005).
3. Liberman, M. C. & Kujawa, S. G. Cochlear synaptopathy in acquired sensorineural hearing loss: manifestations and mechanisms. *Hear. Res.* **349**, 138–147 (2017).
4. Someya, S. *et al.* Sirt3 mediates reduction of oxidative damage and prevention of age-related hearing loss under caloric restriction. *Cell* **143**, 802–812 (2010).
5. Martínez-Vega, R. *et al.* Folic acid deficiency induces premature hearing loss through mechanisms involving cochlear oxidative stress and impairment of homocysteine metabolism. *FASEB J.* **29**, 418–432 (2014).
6. Ohinata, Y., Yamasoba, T., Schacht, J. & Miller, J. M. Glutathione limits noise-induced hearing loss. *Hear. Res.* **146**, 28–34 (2000).
7. Seidman, M. D., Khan, M. J., Bai, U., Shirwany, N. & Quirk, W. S. Biologic activity of mitochondrial metabolites on aging and age-related hearing loss. *Otol. Neurotol.* **21**, 161–167 (2000).
8. Yamasoba, T., Nuttall, A. L., Harris, C., Raphael, Y. & Miller, J. M. Role of glutathione in protection against noise-induced hearing loss. *Brain Res.* **784**, 82–90 (1998).
9. Böttger, E. C. & Schacht, J. The mitochondrion: a perpetrator of acquired hearing loss. *Hear. Res.* **303**, 12–19 (2013).
10. Kim, H.-J. *et al.* NAD+ metabolism in age-related hearing loss. *Aging Dis.* **5**, 150 (2014).
11. Bielefeld, E. C. *et al.* Noise protection with N-acetyl-L-cysteine (NAC) using a variety of noise exposures, NAC doses, and routes of administration. *Acta Otolaryngol.* **127**, 914–919 (2007).
12. Becker, W. *et al.* Fluorescence lifetime imaging by time-correlated single-photon counting. *Microsc. Res. Tech.* **63**, 58–66 (2004).
13. Blacker, T. S. & Duchen, M. R. Characterizing metabolic states using fluorescence lifetime imaging microscopy (FLIM) of NAD(P)H. *NeuroMethods* **123**, (2017).
14. Kolenc, O. I. & Quinn, K. P. Evaluating Cell Metabolism Through Autofluorescence Imaging of NAD (P) H and FAD. *Antioxid. Redox Signal.* (2018).
15. Blacker, T. S. & Duchen, M. R. Investigating mitochondrial redox state using NADH and NADPH autofluorescence. *Free Radic. Biol. Med.* **100**, 53–65 (2016).
16. Schaefer, P. M., Kalinina, S., Rueck, A., von Arnim, C. A. F. & von Einem, B. NADH Autofluorescence—A Marker on its Way to Boost Bioenergetic Research. *Cytom. Part A* (2018).
17. Blacker, T. S., Sewell, M. D. E., Szabadkai, G. & Duchen, M. R. Metabolic Profiling of Live Cancer Tissues Using NAD (P) H Fluorescence Lifetime Imaging. In *Cancer Metabolism* 365–387 (Springer, 2019).

18. Ying, W. NAD⁺/NADH and NADP⁺/NADPH in cellular functions and cell death: regulation and biological consequences. *Antioxid Redox Signal* **10**, 179–206 (2008).
19. Blacker, T. S. *et al.* Separating NADH and NADPH fluorescence in live cells and tissues using FLIM. *Nat. Commun.* **5**, 3936 (2014).
20. Sharick, J. T. *et al.* Protein-bound NAD (P) H Lifetime is Sensitive to Multiple Fates of Glucose Carbon. *Sci. Rep.* **8**, 5456 (2018).
21. Yaseen, M. A. *et al.* Fluorescence lifetime microscopy of NADH distinguishes alterations in cerebral metabolism *in vivo*. *Biomed. Opt. Express* **8**, 2368–2385 (2017).
22. Alam, S. R. *et al.* Investigation of mitochondrial metabolic response to doxorubicin in prostate cancer cells: an NADH, FAD and tryptophan FLIM assay. *Sci. Rep.* **7**, 10451 (2017).
23. Pate, K. T. *et al.* Wnt signaling directs a metabolic program of glycolysis and angiogenesis in colon cancer. *EMBO J.* **33**, 1454–1473 (2014).
24. Blacker, T. S., Marsh, R. J., Duchen, M. R. & Bain, A. J. Activated barrier crossing dynamics in the non-radiative decay of NADH and NADPH. *Chem. Phys.* **422**, 184–194 (2013).
25. Blacker, T. S., Nicolaou, N., Duchen, M. R. & Bain, A. J. Polarised Two-Photon Absorption and Heterogeneous Fluorescence Dynamics in NAD (P) H. *J. Phys. Chem. B* **123**, 4705–4717 (2019).
26. Lagarto, J. *et al.* Application of time-resolved autofluorescence to label-free *in vivo* optical mapping of changes in tissue matrix and metabolism associated with myocardial infarction and heart failure. *Biomed. Opt. Express* **6**, 324–346 (2015).
27. Zholudeva, L. V., Ward, K. G., Nichols, M. G. & Smith, H. J. Gentamicin differentially alters cellular metabolism of cochlear hair cells as revealed by NAD(P)H fluorescence lifetime imaging. *J. Biomed. Opt.* **20**, 051032 (2015).
28. Nickel, A. G. *et al.* Reversal of Mitochondrial Transhydrogenase Causes Oxidative Stress in Heart Failure. *Cell Metab.* **22**, 472–484 (2015).
29. Tosatto, A. *et al.* The mitochondrial calcium uniporter regulates breast cancer progression via HIF-1 α . *EMBO Mol. Med.* **8**, 569–85 (2016).
30. Haythorne, E. *et al.* Diabetes causes marked inhibition of mitochondrial metabolism in pancreatic β -cells. *Nat. Commun.* **10**, 2474 (2019).
31. Majumder, P., Duchen, M. R. & Gale, J. E. Cellular glutathione content in the organ of Corti and its role during ototoxicity. *Front. Cell. Neurosci.* **9**, 143 (2015).
32. Hesse, L. L. *et al.* Non-monotonic relation between noise exposure severity and neuronal hyperactivity in the auditory midbrain. *Front. Neurol.* **7**, 133 (2016).
33. Roth, B. & Bruns, V. Postnatal development of the rat organ of Corti. *Anat. Embryol. (Berl.)* **185**, 571–581 (1992).
34. Blacker, T. S., Berecz, T., Duchen, M. R. & Szabadkai, G. Assessment of Cellular Redox State Using NAD (P) H Fluorescence Intensity and Lifetime. *Bio-protocol* **7**, (2017).
35. Willott, J. F. Effects of aging, hearing loss, and anatomical location on thresholds of inferior colliculus neurons in C57BL/6 and CBA mice. *J. Neurophysiol.* **56**, 391–408 (1986).
36. Miyazawa, H. & Aulehla, A. Revisiting the role of metabolism during development. *Development* **145**, dev131110 (2018).
37. Hequembourg, S. & Liberman, M. C. Spiral ligament pathology: a major aspect of age-related cochlear degeneration in C57BL/6 mice. *JARO-Journal Assoc. Res. Otolaryngol.* **2**, 118–129 (2001).
38. Kane, K. L. *et al.* Genetic background effects on age-related hearing loss associated with Cdh23 variants in mice. *Hear. Res.* **283**, 80–88 (2012).
39. Houtkooper, R. H., Cantó, C., Wanders, R. J. & Auwerx, J. The secret life of NAD⁺: an old metabolite controlling new metabolic signaling pathways. *Endocr. Rev.* **31**, 194–223 (2010).
40. Agledal, L., Niere, M. & Ziegler, M. The phosphate makes a difference: cellular functions of NADP. *Redox Rep.* **15**, 2–10 (2010).
41. Murphy, M. P. How mitochondria produce reactive oxygen species. *Biochem J* **417**, 1–13 (2009).
42. Sies, H. Oxidative stress: a concept in redox biology and medicine. *Redox Biol.* **4**, 180–183 (2015).
43. Corona, J. C., de Souza, S. C. & Duchen, M. R. PPAR γ activation rescues mitochondrial function from inhibition of complex I and loss of PINK1. *Exp. Neurol.* **253**, 16–27 (2014).
44. Keelan, J., Allen, N. J., Antcliffe, D., Pal, S. & Duchen, M. R. Quantitative imaging of glutathione in hippocampal neurons and glia in culture using monochlorobimane. *J. Neurosci. Res.* **66**, 873–84 (2001).
45. Pollak, N., Niere, M. & Ziegler, M. NAD kinase levels control the NADPH concentration in human cells. *J Biol Chem* **282**, 33562–33571 (2007).
46. Nordmann, A. S., Bohne, B. A. & Harding, G. W. Histopathological differences between temporary and permanent threshold shift 1. *Hear. Res.* **139**, 13–30 (2000).
47. Forge, A. Outer hair cell loss and supporting cell expansion following chronic gentamicin treatment. *Hear. Res.* **19**, 171–182 (1985).
48. Kujawa, S. G. & Liberman, M. C. Adding insult to injury: cochlear nerve degeneration after “temporary” noise-induced hearing loss. *J. Neurosci.* **29**, 14077–14085 (2009).
49. Mann, Z. F., Duchen, M. R. & Gale, J. E. Mitochondria modulate the spatio-temporal properties of intra- and intercellular Ca²⁺ signals in cochlear supporting cells. *Cell Calcium* **46**, 136–146 (2009).
50. Sirko, P., Gale, J. E. & Ashmore, J. F. Intercellular Ca²⁺ signalling in the adult mouse cochlea. *J. Physiol.* **597**, 303–317 (2019).
51. Gale, J. E., Piazza, V., Ciubotaru, C. D. & Mammano, F. A mechanism for sensing noise damage in the inner ear. *Curr. Biol.* **14**, 526–529 (2004).
52. Allaman, I., Belanger, M. & Magistretti, P. J. Astrocyte–neuron metabolic relationships: for better and for worse. *Trends Neurosci.* **34**, 76–87 (2011).
53. Shih, A. Y. *et al.* Cystine/glutamate exchange modulates glutathione supply for neuroprotection from oxidative stress and cell proliferation. *J. Neurosci.* **26**, 10514–10523 (2006).
54. Fetoni, A. R. *et al.* Cx26 partial loss causes accelerated presbycusis by redox imbalance and dysregulation of Nfr2 pathway. *Redox Biol.* **19**, 301–317 (2018).
55. Speakman, J. R. & Selman, C. The free-radical damage theory: accumulating evidence against a simple link of oxidative stress to ageing and lifespan. *Bioessays* **33**, 255–259 (2011).
56. Khan, J. Y. & Black, S. M. Developmental changes in murine brain antioxidant enzymes. *Pediatr. Res.* **54**, 77 (2003).
57. Mavelli, I., Rigo, A., Federico, R., Ciriolo, M. R. & Rotilio, G. Superoxide dismutase, glutathione peroxidase and catalase in developing rat brain. *Biochem. J.* **204**, 535–540 (1982).
58. Hussain, S., Slikker, W. Jr. & Ali, S. F. Age-related changes in antioxidant enzymes, superoxide dismutase, catalase, glutathione peroxidase and glutathione in different regions of mouse brain. *Int. J. Dev. Neurosci.* **13**, 811–817 (1995).
59. Delmaghani, S. *et al.* Hypervulnerability to sound exposure through impaired adaptive proliferation of peroxisomes. *Cell* **163**, 894–906 (2015).
60. Skala, M. C. *et al.* *In vivo* multiphoton fluorescence lifetime imaging of protein-bound and free nicotinamide adenine dinucleotide in normal and precancerous epithelia. *J. Biomed. Opt.* **12**, 24014 (2007).
61. Awasthi, K., Moriya, D., Nakabayashi, T., Li, L. & Ohta, N. Sensitive detection of intracellular environment of normal and cancer cells by autofluorescence lifetime imaging. *J. Photochem. Photobiol. B Biol.* **165**, 256–265 (2016).
62. Pastore, M. N., Studier, H., Bonder, C. S. & Roberts, M. S. Non-invasive metabolic imaging of melanoma progression. *Exp. Dermatol.* **26**, 607–614 (2017).

63. Sabharwal, S. S. & Schumacker, P. T. Mitochondrial ROS in cancer: initiators, amplifiers or an Achilles' heel? *Nat. Rev. Cancer* **14**, 709 (2014).
64. Newsholme, P., Cruzat, V. F., Keane, K. N., Carlessi, R. & de Bittencourt, P. I. H. Molecular mechanisms of ROS production and oxidative stress in diabetes. *Biochem. J.* **473**, 4527–4550 (2016).
65. Schaefer, P. M. *et al.* Mitochondrial matrix pH as a decisive factor in neurometabolic imaging. *Neurophotonics* **4**, 45004 (2017).
66. Selivanov, V. A. *et al.* The role of external and matrix pH in mitochondrial reactive oxygen species generation. *J. Biol. Chem.* (2008).
67. Vljakovic, S. M., Lin, S. C., Wong, A. C. Y., Wackrow, B. & Thorne, P. R. Noise-induced changes in expression levels of NADPH oxidases in the cochlea. *Hear. Res.* **304**, 145–152 (2013).
68. Koshkin, V., Lotan, O. & Pick, E. Electron transfer in the superoxide-generating NADPH oxidase complex reconstituted *in vitro*. *Biochim. Biophys. Acta (BBA)-Bioenergetics* **1319**, 139–146 (1997).
69. Gorrini, C., Harris, I. S. & Mak, T. W. Modulation of oxidative stress as an anticancer strategy. *Nat. Rev. Drug Discov.* **12**, 931 (2013).
70. Diehn, M. *et al.* Association of reactive oxygen species levels and radioresistance in cancer stem cells. *Nature* **458**, 780 (2009).
71. Landriscina, M., Maddalena, F., Laudiero, G. & Esposito, F. Adaptation to oxidative stress, chemoresistance, and cell survival. *Antioxid. Redox Signal.* **11**, 2701–2716 (2009).
72. Traverso, N. *et al.* Role of glutathione in cancer progression and chemoresistance. *Oxid. Med. Cell. Longev.* **2013**, (2013).
73. Majumder, P., Moore, P. A., Richardson, G. P. & Gale, J. E. Protecting mammalian hair cells from aminoglycoside-toxicity: Assessing phenoxybenzamine's potential. *Front. Cell. Neurosci.* **11**, 94 (2017).
74. Chouchani, E. T. *et al.* Ischaemic accumulation of succinate controls reperfusion injury through mitochondrial ROS. *Nature* **515**, 431–5 (2014).

Acknowledgements

PM was supported by an Action On Hearing Loss Pauline Ashley award (PA12), a Conselho Nacional de Desenvolvimento Científico e Tecnológico (CNPq) fellowship (249335/2013-1) and by an Action On Hearing Loss International Grant (G52) and Flexi-grant (F66). TSB acknowledges funding from BBSRC grants BB/L020874/1 and BB/P018726/1, in addition to the Prof. Anne Warner Doctoral Fellowship awarded by UCL CoMPLEX. We are grateful to Prof. Mathias Ziegler (University of Bergen, Norway) for gifting the NADK+ HEK293 cell line.

Author contributions

All authors contributed to the initial conception and design of the work. P.M. and T.S.B. undertook experiments and data analysis. L.N. performed the noise exposure protocol. All authors drafted the manuscript.

Competing interests

The authors declare no competing interests.

Additional information

Supplementary information is available for this paper at <https://doi.org/10.1038/s41598-019-55329-x>.

Correspondence and requests for materials should be addressed to P.M. or T.S.B.

Reprints and permissions information is available at www.nature.com/reprints.

Publisher's note Springer Nature remains neutral with regard to jurisdictional claims in published maps and institutional affiliations.



Open Access This article is licensed under a Creative Commons Attribution 4.0 International License, which permits use, sharing, adaptation, distribution and reproduction in any medium or format, as long as you give appropriate credit to the original author(s) and the source, provide a link to the Creative Commons license, and indicate if changes were made. The images or other third party material in this article are included in the article's Creative Commons license, unless indicated otherwise in a credit line to the material. If material is not included in the article's Creative Commons license and your intended use is not permitted by statutory regulation or exceeds the permitted use, you will need to obtain permission directly from the copyright holder. To view a copy of this license, visit <http://creativecommons.org/licenses/by/4.0/>.

© The Author(s) 2019